

# Preparation, characterization, and utilization of multi-functional magnetic-fluorescent composites for bio-imaging and magnetic hyperthermia therapy†

Cite this: *RSC Advances*, 2013, **3**, 7838

Supparesk Rittikulsittichai,<sup>a</sup> Burapol Singhana,<sup>a</sup> William W. Bryan,<sup>a</sup> Subhasis Sarangi,<sup>c</sup> Andrew C. Jamison,<sup>a</sup> Audrius Brazdeikis<sup>\*bc</sup> and T. Randall Lee<sup>\*ac</sup>

This paper describes the synthesis, characterization, and utilization of unique multi-functional magnetic composites that integrate optical and magnetic properties in a single structure for use in hyperthermia therapy, and magnetic and fluorescence imaging. The composites are comprised of nanoscale magnetic core particles that are encapsulated by a silica layer that contains covalently-embedded organic dyes. The morphologies of the nanocomposite particles were characterized by TEM and FE-SEM. Their optical and magnetic properties were evaluated by spectrofluorometry and SQUID magnetometry, respectively. The results demonstrate that the nanocomposites are monodisperse and uniformly spherical with well-defined shell-core structures; moreover, they exhibit high magnetic saturation, produce vivid fluorescence, and can be designed to provide exceptional stability in aqueous solution over a wide range of pH and at elevated temperatures. For the three dyes utilized in the synthesis of these composites, rhodamine B (RhB), fluorescein (Flu), and 7-hydroxycoumarin (Cou), the observed relative stability for the nanoparticles was: RhB-SiO<sub>2</sub>-Fe<sub>3</sub>O<sub>4</sub> > Flu-SiO<sub>2</sub>-Fe<sub>3</sub>O<sub>4</sub> > Cou-SiO<sub>2</sub>-Fe<sub>3</sub>O<sub>4</sub>. Additionally, potential uses of these composite nanoparticles as bimodal contrast agents and therapeutic entities are demonstrated.

Received 9th January 2013,  
Accepted 5th March 2013

DOI: 10.1039/c3ra41002a

[www.rsc.org/advances](http://www.rsc.org/advances)

## Introduction

The development of noninvasive diagnostic imaging modalities and living-tissue imaging has attracted considerable attention in recent years. An optical imaging technique based on fluorescent contrast agents is a relatively simple procedure that offers excellent resolution, high sensitivity, and rapid scan times.<sup>1,2</sup> This technique, however, is currently unable to provide cross-sectional images. Furthermore, scanning probe techniques such as atomic/magnetic force microscopy afford images of nanoparticles with a high spatial resolution but with limited practical clinical applications. Superparamagnetic nanoparticles are used in standard clinical imaging and emerging imaging applications such as contrast enhanced magnetic resonance imaging (MRI),<sup>3–6</sup> magnetic particle imaging (MPI),<sup>7,8</sup> and magnetic relaxation imaging (MRXI).<sup>9,10</sup> More recently, the use of magnetic nanoparticles has been shown to be a promising approach for guided surgery and radiation-free sentinel lymph node mapping.<sup>11,12</sup> Sentinel

lymph nodes can also be mapped using contrast enhanced MRI techniques, but this application does not allow probe-guided surgery.<sup>13</sup> Combining magnetic and optical properties into one multifunction particle allows the development of multimodal imaging technologies that provide more complementary data sets than any isolated imaging agent.<sup>14–20</sup> Moreover, the magnetic properties allow localization, manipulation, and/or heating of magnetic-fluorescent nanoparticles for developing a new array of medical tools and devices for guided intervention and therapeutics.<sup>17,21–29</sup>

Currently, several approaches are used to fabricate magnetic-fluorescent composite nanoparticles.<sup>17–19,25–28,30–38</sup> One general route of preparation involves the encapsulation of a magnetic core within a silica shell containing an organic fluorescent dye.<sup>19,20,26,39–43</sup> The silica layer serves as a coating material that can limit the aggregation of the nanoparticles, enhance their stability in aqueous solution, and also render the nanoparticles biocompatible.<sup>44,45</sup> Furthermore, an organic fluorescent dye can be directly incorporated into the silica matrix without quenching the fluorescent properties.<sup>26,42</sup> However, some loss of signal for embedded dyes has been reported and attributed to an interaction with the iron oxide core.<sup>20</sup> Importantly, embedding the dye within the silica matrix can prevent leaching from the composite nanoparticles, thereby yielding stable fluorescent signals.<sup>42</sup> Additionally, the silica surfaces of encapsulated magnetic nanoparticles can be

<sup>a</sup>Department of Chemistry, University of Houston, 4800 Calhoun Road, Houston, Texas 77204-5003 E-mail: trlee@uh.edu

<sup>b</sup>Department of Physics, University of Houston, 4800 Calhoun Road, Houston, Texas 77204-5003

<sup>c</sup>The Texas Center for Superconductivity, University of Houston, 4800 Calhoun Road, Houston, Texas 77204-5003

† Electronic supplementary information (ESI) available. See DOI: 10.1039/c3ra41002a

easily modified by various functional groups using well established silane chemistry.<sup>46</sup>

Due to their photostability and facile derivitization, rhodamine isothiocyanate (RITC) and fluorescein isothiocyanate (FITC) are two fluorescent dyes that have been embedded within silica matrices. In particular, their isothiocyanate moiety can be readily coupled with the amine groups of compounds such as 3-aminopropyltriethoxysilane (APTES) *via* thiourea linkages.<sup>47,48</sup> The modified fluorescent dyes can be entrapped in silica matrices *via* co-precipitated condensation with tetraethyl orthosilicate (TEOS) during the course of the growth of the silica shell around the magnetic cores.<sup>20,26,39–43</sup> However, among several drawbacks,<sup>47,49,50</sup> colloidal particles prepared *via* this strategy are stable only over narrow pH ranges; specifically, since the primary amine group terminated on the surface of a silica-nanocomposite can tolerate and maintain a colloidal dispersion only under acidic conditions, the particles readily precipitate under neutral and basic conditions. We note also that most previous methods employ relatively small magnetic nanoparticles (2–8 nm in diameter) encapsulated within the dye-doped silica coating, which allows only weak magnetic responses ( $M_s \leq 5 \text{ emu g}^{-1}$ ),<sup>19,26,39,40,43</sup> which is problematic since the response to a magnetic field decreases with distance. In applications, the remote manipulation of small magnetic nanoparticles at the desired target site, along with maintaining their proximity to the desired target (*i.e.*, inflammatory or tumor sites) in the face of blood circulation, using an external magnetic gradient is consequently restricted.<sup>49</sup> Another drawback of small magnetic nanoparticles with weak saturation magnetization is that the particles fail to generate sufficient heat when exposed to an external alternating magnetic field, which also limits their utility as a therapeutic agent in hyperthermia therapy.<sup>50,51</sup> Furthermore, the silica/dye coating process can lead to irregular core-shell structures or aggregates.<sup>18,30,39–42</sup> Collectively, these factors limit the use of such composite nanoparticles in biomedical applications.

Importantly, magnetic particles and/or magnetic composites that range in diameter from sub-micrometer to micrometer sizes not only exhibit high values of magnetization but also a dynamic response to an external magnetic field, thus generating sufficient heat for hyperthermia applications.<sup>52–57</sup> These magnetic composites have become widely used to introduce a drug or perform a therapeutic task by accumulation in the inflammatory site with the aid of a magnetic field.<sup>58–64</sup> Depending on the architecture of the composite particle, drugs can be released by several mechanisms, including radiation<sup>59</sup> or changes in environmental temperature. Additionally, drug release can be magnetically triggered.<sup>65–67</sup>

Consequently, the development of magnetic-fluorescent composites that exhibit robust stability over a wide range of pH values (both acidic to basic), uniform size distributions, and high magnetic responses, are needed to advance the emerging fields of nanotechnology-based diagnosis, imaging, and therapy. To this end, we report here a unique class of

magnetic-fluorescent composite nanoparticle for use in drug delivery, hyperthermia therapy, and magnetic and fluorescent imaging, which exhibits high magnetization, vivid fluorescence, and unprecedented stability over a wide range of pH. Our approach derives from the strategy reported by Lee and co-workers that affords fluorescent silica nanoparticles with no magnetic core.<sup>68</sup> In contrast, we encapsulate large magnetic nanoparticles ( $\sim 118 \text{ nm}$  diameter) within a porous silica shell layer, in which fluorescent dye molecules are covalently anchored within the shell pores. The resultant fluorescent dye-labeled silica-shell-magnetic-core composites (dye-SiO<sub>2</sub>-Fe<sub>3</sub>O<sub>4</sub>) are monodisperse and uniformly spherical with well-defined core-shell structures. Furthermore, this study shows how dye-SiO<sub>2</sub>-Fe<sub>3</sub>O<sub>4</sub> nanoparticles can be prepared to exhibit high magnetic saturation, produce vivid fluorescence, and remain stable in solution after exposure to elevated temperatures. The optical properties of these hybrid nanoparticles are tunable by judiciously choosing and appropriately modifying the fluorescent dyes to be incorporated into the silica matrix. Moreover, the covalent bonds between the dye and the silica matrix can prevent an appropriately designed dye from detaching from the composite nanoparticle,<sup>68</sup> giving rise to multifunctional hybrid nanoparticles that exhibit stable fluorescent signals. We anticipate that these new magnetic-fluorescent nanocomposites will serve as effective agents for multimodal diagnostic imaging, hyperthermic therapeutics, and nanoscale drug delivery.

## Experimental section

### Materials

The following chemicals were obtained from the indicated suppliers and used as received: sodium acetate anhydrous (Mallinckrodt Baker) and iron(III) chloride hexahydrate (FeCl<sub>3</sub>·6H<sub>2</sub>O, Alfa Aesar). Ammonium hydroxide (30% NH<sub>3</sub> in H<sub>2</sub>O), sodium hydroxide (NaOH), ethylene glycol (EG) and ethanol were obtained from EM Science. Cesium carbonate, Pt on activated charcoal, platinum(0)-1,3-divinyl-1,1,3,3-tetra-methylsiloxane complex solution (Pt(dvs)), rhodamine B, fluorescein, 7-hydroxycoumarin, trimethoxysilane (TMS, 98%), tetraethylorthosilicate (TEOS, 98%), and polyvinylpyrrolidone (PVP,  $M_w \sim 15\,000$ ) were obtained from Aldrich. Commercial magnetite nanoparticle samples (nanomag<sup>®</sup>-D) were obtained from Micromod. The Milli-Q water used throughout all reactions was purified to a resistance of 18 MΩ cm and filtered through a 0.22 μm filter membrane to remove any impurities. All glassware and equipment were cleaned in an aqua regia solution and rinsed with Milli-Q water prior to use (Academic Milli-Q Water System; Millipore Corporation).

### Synthesis of trialkoxysilane-modified rhodamine B, fluorescein, and 7-hydroxycoumarin

The trialkoxysilane-modified dyes, rhodamine B (RhB), fluorescein (Flu), and 7-hydroxycoumarin (Cou), were synthesized using the procedure reported by Lee and co-workers.<sup>68</sup>

### Synthesis of Fe<sub>3</sub>O<sub>4</sub> nanoparticles

The magnetic Fe<sub>3</sub>O<sub>4</sub> nanoparticles were synthesized *via* straightforward modification of a procedure reported by Li and co-workers.<sup>69</sup> In this modified procedure, a round-bottomed flask was charged with FeCl<sub>3</sub>·6H<sub>2</sub>O (2.0 g), which was then dissolved in 15 mL ethylene glycol followed by the addition of sodium acetate (5.4 g). The latter addition led to a rapid change in the color of the solution from orange to brown. The solution was stirred for an additional 30 min and then injected at once into a round-bottomed flask containing a vigorously stirred solution of PVP (0.60 g) in 60 mL ethylene glycol heated to 180 °C. The mixture was then vigorously stirred at 180 °C for 8 h. After cooling the solution to room temperature, the resulting black precipitate was collected using a bar magnet. The nanoparticles were purified by repeated cycles of washing and redispersing in ethanol and Milli-Q water.

### Synthesis of fluorescent dye-labeled silica/magnetic spheres

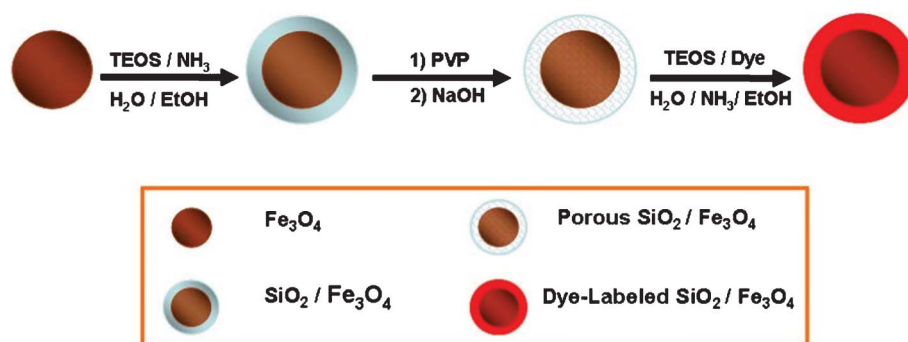
The preparation of the dye-SiO<sub>2</sub>-Fe<sub>3</sub>O<sub>4</sub> nanoparticles includes three main steps. First, the surface of the magnetic sphere was initially coated with a thin silica shell using a modification of a procedure reported by Stöber *et al.*<sup>70</sup> In this modification, 0.075 g of the magnetic spheres described above were redispersed into a mixed solution of ammonia (3.0 mL), Milli-Q water (6.0 mL), and ethanol (60.0 mL). The resulting solution was mechanically stirred for 5 min, after which TEOS (0.3 mL) was added. The mixture was then further stirred overnight at rt to afford magnetic nanoparticles encapsulated by a thin silica shell; these nanoparticles can be isolated using a bar magnet and purified by washing with copious amounts of ethanol before dispersing in 60 mL water. Second, the surface of the silica layer was made porous using a procedure reported by Yin and co-workers.<sup>71</sup> Typically, the above described colloidal solution was mixed with PVP (3 g) and brought to reflux for 3 h. After cooling the solution to rt, 15 mL NaOH solution (0.16 g mL<sup>-1</sup>) was injected into the mixture to initiate the etching process, and the mixture was vigorously stirred for 90 additional min. The composite particles with a porous outer silica shell were isolated from the basic solution using a bar magnet and purified by washing with deionized water several times. Thereafter, the resultant nanoparticles were dispersed in 20 mL deionized water. Finally, covalent

incorporation of the dye was achieved by dispersing the above colloidal solution (3 mL) into ethanol (20 mL) and concentrated ammonia solution (1 mL). The trialkoxysilane-modified fluorescent dye (1 mL; 4 mg mL<sup>-1</sup> in ethanol) and TEOS (0.1 mL) were then gradually added to the mixture. The reaction was allowed to proceed for 12 h at rt under vigorous stirring. The resulting nanoparticles were then magnetically separated and repeatedly washed with ethanol and deionized water several times to remove any residual impurities.

### Nanoparticle characterization

The morphology of the composite nanoparticles was evaluated using a LEO-1525 scanning electron microscope (SEM) operating at 15 kV. To obtain high resolution SEM images, all samples were deposited on a silicon wafer. Similarly, the particle size and morphology were also evaluated by employing a JEM-2000 FX transmission electron microscope (TEM) operating at an accelerating voltage of 200 kV. All TEM samples were deposited on a 300 mesh holey carbon-coated copper grid and dried overnight before analysis. The structure of the magnetic Fe<sub>3</sub>O<sub>4</sub> spheres was confirmed by an X-ray powder diffractometer (Scintag XDS 2000) with monochromatic Cu-K $\alpha$  radiation ( $\lambda = 1.540562$  Å) and a step size of 0.02°. The SEM and TEM images, along with other characterization data for these nanoparticles, can be found in Fig. S1 and S2 in the supporting information.†

The magnetic properties were evaluated by employing a vibrating sample magnetometer (VSM) at room temperature. The magnetic images of hybrid dye-SiO<sub>2</sub>-Fe<sub>3</sub>O<sub>4</sub> nanoparticles were obtained by measuring the dynamic susceptibility using a hand-held magnetic probe similar to an intraoperative sensing probe used in magnetic nanoparticle-guided surgery. A droplet of the dye-SiO<sub>2</sub>-Fe<sub>3</sub>O<sub>4</sub> colloid was deposited onto a standard glass slide and allowed to dry for 30 min, forming a thin uniform layer of approximately 200  $\mu$ g Fe. The glass slide with dry thin samples was mounted 2 mm under the tip of the probe, and magnetic 2D images were obtained by moving the slide using a computer-controlled XY scanning stage. The typical scanning area was 60  $\times$  60 mm and the step size was 0.1 mm. The diameter of the sensing probe was 6 mm. An alternating current (AC) drive magnetic field of 2 kHz was applied, causing a time-dependent moment in the thin-film sample. The field of the time-dependent moment induced a



**Scheme 1** Strategy for the fabrication of magnetic-fluorescent composite nanoparticles.

current in the pickup coils, which was detected by a remotely located HTS SQUID sensor.

The magnetic susceptibility image of the dye-SiO<sub>2</sub>-Fe<sub>3</sub>O<sub>4</sub> nanoparticles was compared with commercially available magnetite magnetic nanoparticles (nanomag<sup>®</sup>-D, Micromod). These magnetic nanoparticles are composed of a core of iron oxide nanocrystals encapsulated in a dextran matrix and coated with polyethylene glycol (PEG) to prevent agglomeration. They have an average diameter of 130 nm, a polydispersity index of <0.2, and a saturation magnetization of >67 emu g<sup>-1</sup>.

The fluorescence spectra of RhB, Flu, Cou, RhB-SiO<sub>2</sub>-Fe<sub>3</sub>O<sub>4</sub>, Flu-SiO<sub>2</sub>-Fe<sub>3</sub>O<sub>4</sub>, and Cou-SiO<sub>2</sub>-Fe<sub>3</sub>O<sub>4</sub> were recorded with a SPF-500C spectrofluorometer. For the fluorescent optical images, the nanoparticles were deposited on a glass slide and were visualized using a Nikon H600L microscope system in normal brightfield mode and fluorescence mode.

To test the photostability of the composite nanoparticles, ethanolic solutions of RhB-SiO<sub>2</sub>-Fe<sub>3</sub>O<sub>4</sub>, Flu-SiO<sub>2</sub>-Fe<sub>3</sub>O<sub>4</sub>, Cou-SiO<sub>2</sub>-Fe<sub>3</sub>O<sub>4</sub>, RhB, Flu, and Cou were individually exposed

under a mercury discharge lamp (160 W). The fluorescent intensities of all samples were evaluated in 30 min intervals for 120 min of light exposure.

To evaluate the detachment of the dyes from the composite nanoparticles at elevated temperatures, colloidal solutions of dye-SiO<sub>2</sub>-Fe<sub>3</sub>O<sub>4</sub> nanoparticles were refluxed in a copious volume of deionized water and ethanol for 24 h. After refluxing, the nanoparticles were collected by centrifugation and then redispersed in deionized water and ethanol. The fluorescent spectra of the colloidal solutions of dye-SiO<sub>2</sub>-Fe<sub>3</sub>O<sub>4</sub> before and after reflux, and that of their supernatant solutions, were recorded.

To evaluate the capacity of the magnetic-fluorescent nanoparticles to induce heat, magnetic hyperthermia experiments were conducted using a 1.2 kW custom-made electromagnetic field generator built around an *N*-channel power MOSFET, Xantrex XRF DC power supply, and an Agilent 33120A function generator to produce an alternating magnetic field having an amplitude 0–10 kA m<sup>-1</sup> at a frequency 60–400 kHz. The dye-SiO<sub>2</sub>-Fe<sub>3</sub>O<sub>4</sub> colloidal samples (0.5 mL) were

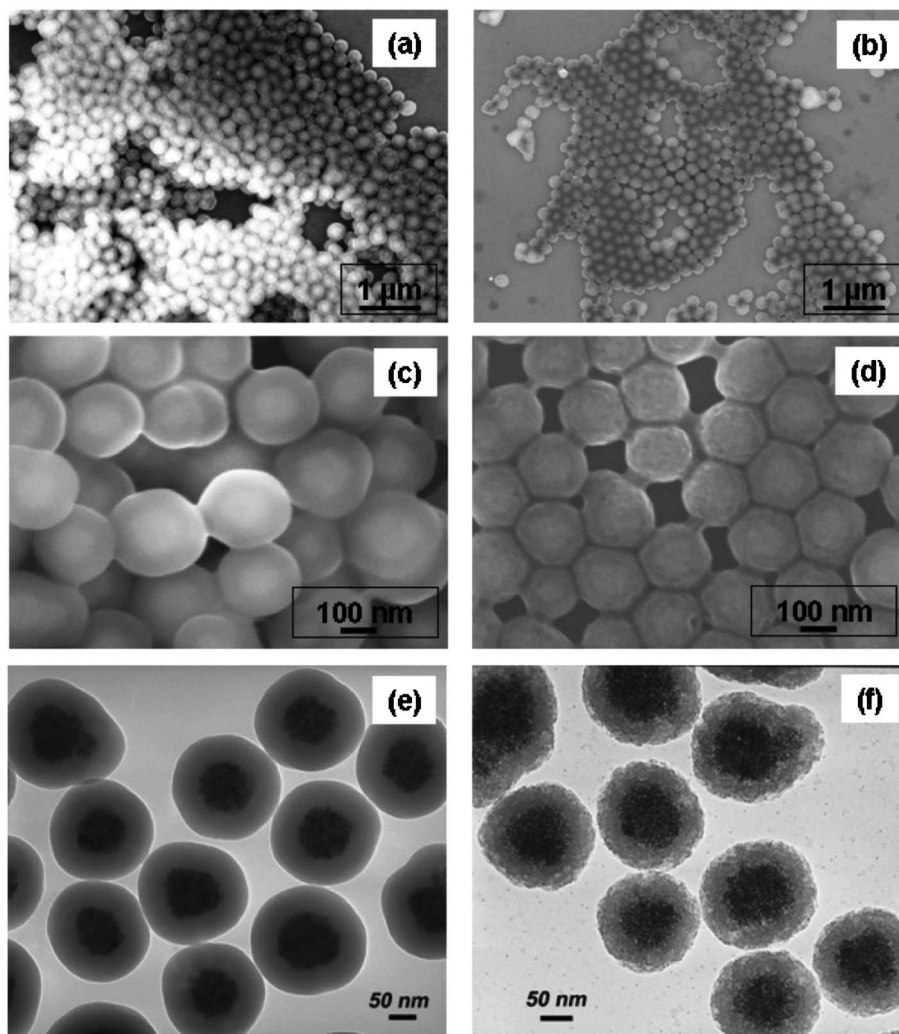


**Fig. 1** Left column: morphology of the SiO<sub>2</sub>-shell-Fe<sub>3</sub>O<sub>4</sub>-core structure imaged by FE-SEM at different magnifications (a, c) and TEM (e). Right column: morphology of porous SiO<sub>2</sub>-shell-Fe<sub>3</sub>O<sub>4</sub>-core structure imaged by FE-SEM at different magnifications (b, d), and TEM (f).

placed inside an induction coil. The coil was tuned to 100 kHz using a matching network. A high density foam insert was used to reduce direct heat transfer from the coil to the sample. The temperature of the colloid was measured every 1 s using a fiber optic temperature sensor (Neoptix) having a temperature resolution of 0.1 °C. To minimize the temperature changes due to Joule heating, the induction coil temperature was stabilized at 34 °C ( $\pm 0.2$  °C) by a thermoelectric water cooler/heater setup.

## Results and discussion

Scheme 1 shows the strategy used to prepare the targeted magnetic-fluorescent nanocomposites. In the first step, we encapsulated magnetic spheres ( $118 \pm 15$  nm in diameter) within an amorphous silica layer ( $\sim 50$  nm thick). We then converted the silica layer to a porous structure because we wished to enhance the dye-loading capacity of the silica layer in order to generate composite nanoparticles with intense fluorescent signals.<sup>20,71–73</sup> Additionally, the porous silica layer can act as a spacer to prevent direct contact between the  $\text{Fe}_3\text{O}_4$  cores and the fluorescent dye molecules, thus reducing any quenching effects by the  $\text{Fe}_3\text{O}_4$  cores.<sup>74</sup> In the final step, we used the base-catalyzed co-hydrolysis of TEOS and a trialkoxysilane-modified dye to covalently embed the fluorescent dye molecules within the silica matrix. The use of excess TEOS in a molar ratio to the modified dye leads to a silica-enriched outermost layer and helps to prevent the dye from leaching from the formerly porous matrix.

### Morphologies and sizes of composite nanoparticles

We characterized the size and morphology of the magnetic composite nanoparticles using SEM and TEM. After being encapsulated within silica, a uniform  $\text{SiO}_2$ -shell- $\text{Fe}_3\text{O}_4$ -core structure was obtained where the shell thickness was  $\sim 50$  nm, as illustrated in Fig. 1a, 1c and 1e. An aqueous solution of NaOH was then added to the colloidal solution to initiate formation of the porous silica layer. After the etching process, the thickness of the silica layer was slightly shrunk from  $\sim 50$  nm to  $\sim 35$  nm. The outermost silica layer became rougher with respect to its initial morphology, thus confirming that the dense silica layer was converted to a porous structure, as indicated by the SEM and TEM images in Fig. 1d and 1f, respectively.

Custom-designed trialkoxysilane-modified dye molecules can be covalently incorporated into the porous silica layer by co-hydrolysis with TEOS, producing a magnetic-fluorescent composite nanoparticle. The SEM and TEM images in Fig. 2a–c of the composite nanoparticles reveal a uniform spherical structure ( $\sim 340$  nm in diameter) with a smooth dye-doped silica shell ( $\sim 110$  nm in thickness). In addition, the fluorescent properties of the composite nanoparticles can be tuned by simply altering the nature of the custom-designed trialkoxysilane-modified dye molecules through judicious synthetic modifications.

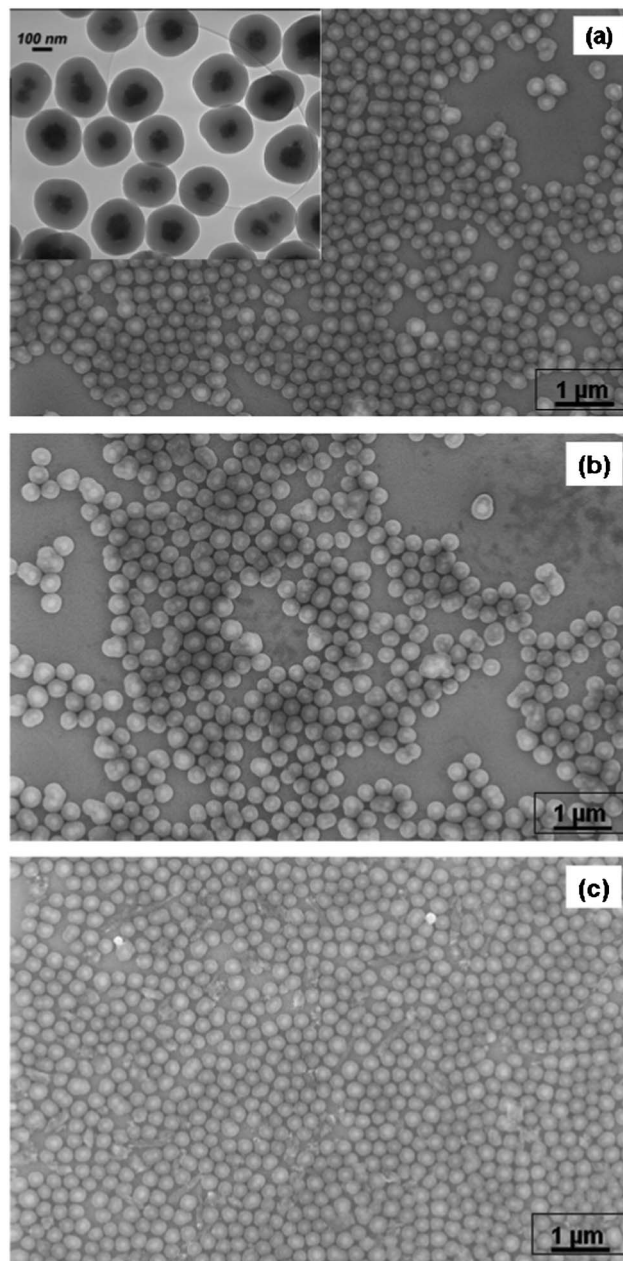
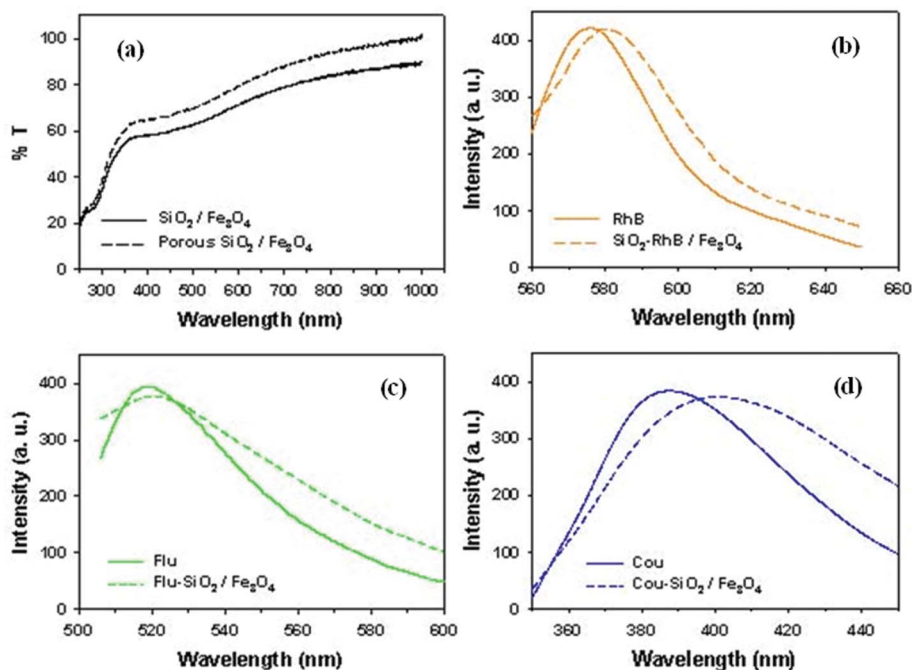


Fig. 2 SEM images of (a) RhB- $\text{SiO}_2$ - $\text{Fe}_3\text{O}_4$ , (b) Flu- $\text{SiO}_2$ - $\text{Fe}_3\text{O}_4$  and (c) Cou- $\text{SiO}_2$ - $\text{Fe}_3\text{O}_4$ . The inset in (a) shows a typical TEM image of RhB- $\text{SiO}_2$ - $\text{Fe}_3\text{O}_4$ .

### Optical properties and fluorescent images of Dye- $\text{SiO}_2/\text{Fe}_3\text{O}_4$ nanoparticles

Fig. 3a shows the UV-vis transmission spectra of silica-coated  $\text{Fe}_3\text{O}_4$  nanoparticles and porous silica-coated  $\text{Fe}_3\text{O}_4$  nanoparticles in aqueous solution at identical concentrations. As indicated by the spectra, the colloidal solution of the porous- $\text{SiO}_2$ - $\text{Fe}_3\text{O}_4$  particles is more transparent than its precursor ( $\text{SiO}_2$ - $\text{Fe}_3\text{O}_4$ ), thereby minimizing any potential interference with incorporated dye molecules. In related work, Fig. 3b–d show the emission spectra of aqueous solutions of the modified dyes (RhB, Flu, and Cou) and the corresponding dye- $\text{SiO}_2$ - $\text{Fe}_3\text{O}_4$  composite nanoparticles. The excitation wave-



**Fig. 3** (a) UV-vis transmission spectra of aqueous solutions of  $\text{SiO}_2\text{-Fe}_3\text{O}_4$  and porous  $\text{SiO}_2\text{-Fe}_3\text{O}_4$ . The emission spectra of aqueous solutions of the modified dyes and the corresponding dye- $\text{SiO}_2\text{-Fe}_3\text{O}_4$  composite nanoparticles: (b) RhB, RhB- $\text{SiO}_2\text{-Fe}_3\text{O}_4$ ; (c) Flu, Flu- $\text{SiO}_2\text{-Fe}_3\text{O}_4$ ; and (d) Cou, Cou- $\text{SiO}_2\text{-Fe}_3\text{O}_4$ .

lengths and emission band maxima of the samples are summarized in Table 1. A comparison of Fig. 3b–d reveals that the emission bands of the colloidal solutions were slightly red shifted with respect to those of the corresponding dyes dissolved in solution. These results can be attributed to the interaction and/or aggregation of dye molecules embedded in the silica matrix.<sup>75</sup>

In further studies, the dye- $\text{SiO}_2\text{-Fe}_3\text{O}_4$  nanoparticles were deposited on a glass slide and imaged using a NIKON H600L microscope system in normal brightfield and fluorescence modes. Fig. 4 shows the brightfield and fluorescence images for the dye- $\text{SiO}_2\text{-Fe}_3\text{O}_4$  nanoparticles. Importantly, the nanoparticles emitted a strong fluorescent color that was consistent with the position of their emission maxima shown in Fig. 3b–d.

The photostability of the dye- $\text{SiO}_2\text{-Fe}_3\text{O}_4$  nanoparticles, as determined by their fluorescence upon exposure to a high intensity discharge lamp, was also examined. Fig. 5 shows the plot of the fluorescent intensities of both the trialkoxysilane-

modified dyes and the dye- $\text{SiO}_2\text{-Fe}_3\text{O}_4$  nanoparticles *versus* illumination time. With this experiment, the fluorescent intensities of the trialkoxysilane-modified dyes uniformly dropped to 50–60% of their initial intensities, while those of the dye- $\text{SiO}_2\text{-Fe}_3\text{O}_4$  nanoparticles proved to retain a greater percentage of their initial fluorescent intensity after being illuminated for 120 min (85–95% of their initial intensities).

The stability of the dye- $\text{SiO}_2\text{-Fe}_3\text{O}_4$  nanoparticles was further investigated to determine their ability to withstand exposure to elevated temperatures. For this procedure, the emission spectra were recorded before and after the dye- $\text{SiO}_2\text{-Fe}_3\text{O}_4$  nanoparticles were refluxed using either ethanol or water as the solvent in separate reflux experiments, as shown in Fig. 6. To obtain the fluorescence spectra after the reflux procedure, the nanoparticles were isolated from the solvent by centrifugation and then redispersed in ethanol. The emission spectra of the separated reflux solvents, the supernatant solutions, for all three types of nanoparticles were also collected, as shown in Fig. 6.

The fluorescent intensities of the RhB- $\text{SiO}_2\text{-Fe}_3\text{O}_4$  and Flu- $\text{SiO}_2\text{-Fe}_3\text{O}_4$  nanoparticles were only minimally changed after exposure to elevated temperatures while in the ethanolic solution, and their supernatant solutions (collected by centrifugation after reflux) showed little indication of a transfer of these fluorescent dyes to the solution. These results illustrate that for the RhB- $\text{SiO}_2\text{-Fe}_3\text{O}_4$  and Flu- $\text{SiO}_2\text{-Fe}_3\text{O}_4$  nanoparticles, the porous silica shells are capable of retaining covalently attached dye molecules in a harsh environment. However, the Cou- $\text{SiO}_2\text{-Fe}_3\text{O}_4$  nanoparticles proved to be less stable compared to the RhB- $\text{SiO}_2\text{-Fe}_3\text{O}_4$  and Flu- $\text{SiO}_2\text{-Fe}_3\text{O}_4$  nanoparticles. The fluorescent intensity of the Cou- $\text{SiO}_2\text{-Fe}_3\text{O}_4$  nanoparticles decreased, while its supernatant exhibited a

**Table 1** Summary of the excitation wavelengths and maximum emission bands of the modified dyes and the dye- $\text{SiO}_2\text{-Fe}_3\text{O}_4$  nanoparticles

	excitation wavelength (nm)	maximum emission bands
RhB	540	576
RhB- $\text{SiO}_2\text{-Fe}_3\text{O}_4$	540	580
Flu	495	518.5
Flu- $\text{SiO}_2\text{-Fe}_3\text{O}_4$	495	520
Cou	340	390
Cou- $\text{SiO}_2\text{-Fe}_3\text{O}_4$	340	397

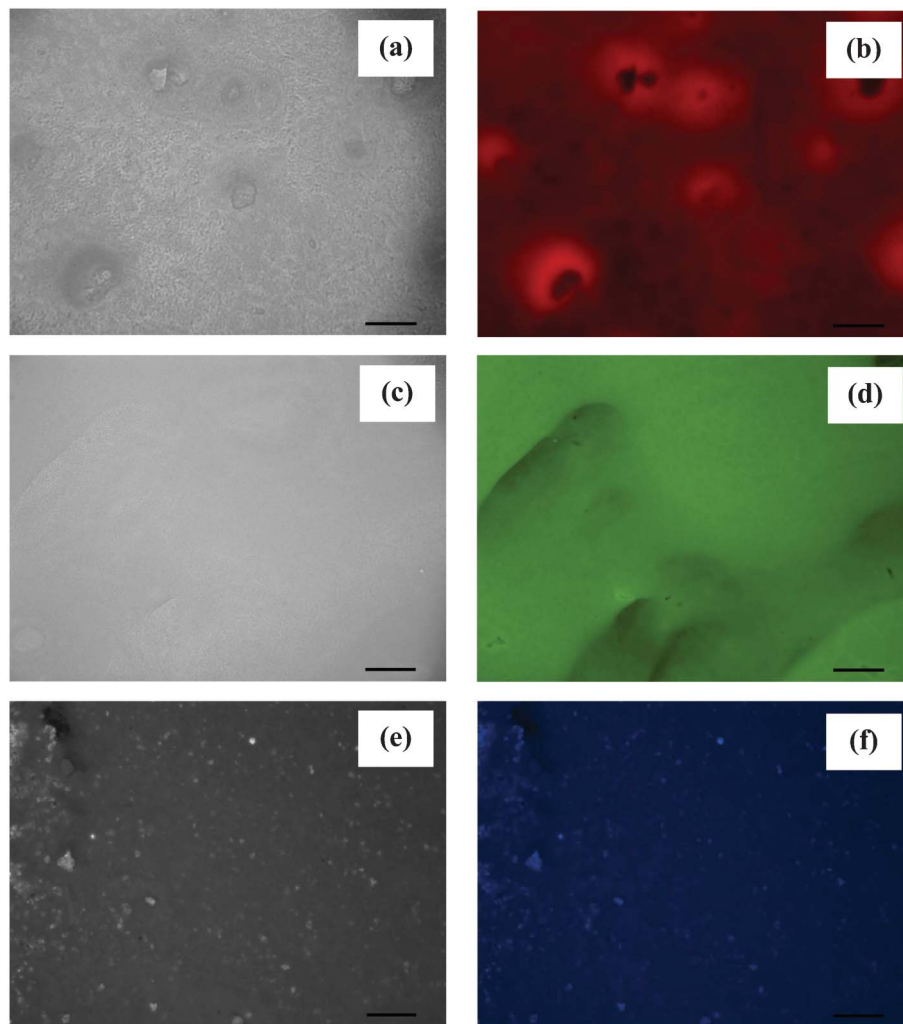


**Fig. 4** NIKON H600L microscope images in normal brightfield mode (a, c, and e) and fluorescent mode (b, d, and f) of RhB-SiO<sub>2</sub>-Fe<sub>3</sub>O<sub>4</sub>, Flu-SiO<sub>2</sub>-Fe<sub>3</sub>O<sub>4</sub>, and Cou-SiO<sub>2</sub>-Fe<sub>3</sub>O<sub>4</sub>, respectively. All scale bars are 50 μm.

strong fluorescent intensity. These results clearly indicate that there was some quantity of modified-Coumarin dye being released from the silica matrix while dissolved in the ethanolic solution during the course of the reflux. Additionally, the high fluorescent intensity of the Cou-SiO<sub>2</sub>-Fe<sub>3</sub>O<sub>4</sub> nanoparticle solution before being refluxed is attributed to the absence of photo-bleaching effects from the Fe<sub>3</sub>O<sub>4</sub> cores and the strong fluorescent property of the fluorescent dye moiety.<sup>20</sup> When using water as the solvent for reflux, both the Flu-SiO<sub>2</sub>-Fe<sub>3</sub>O<sub>4</sub> and Cou-SiO<sub>2</sub>-Fe<sub>3</sub>O<sub>4</sub> nanoparticles in solution exhibited a large decrease in fluorescence. Only the RhB-SiO<sub>2</sub>-Fe<sub>3</sub>O<sub>4</sub> nanoparticles exhibit a strong retention of the attached dyes in both solvents (see also Fig. S3 in the ESI†). These results point to the following decreasing stability trend for the dye-SiO<sub>2</sub>-Fe<sub>3</sub>O<sub>4</sub> nanoparticles: RhB-SiO<sub>2</sub>-Fe<sub>3</sub>O<sub>4</sub> > Flu-SiO<sub>2</sub>-Fe<sub>3</sub>O<sub>4</sub> > Cou-SiO<sub>2</sub>-Fe<sub>3</sub>O<sub>4</sub>. Notably, this trend also follows the trend for decreasing steric bulk of the dye molecules, as shown in Fig. 7, which might suggest that the presence of a bulky structure above the dye attachment site on the silica surface helps reduce chemical attack at the bonding site. If steric hindrance plays a key role in stabilizing the dye-SiO<sub>2</sub>-Fe<sub>3</sub>O<sub>4</sub>

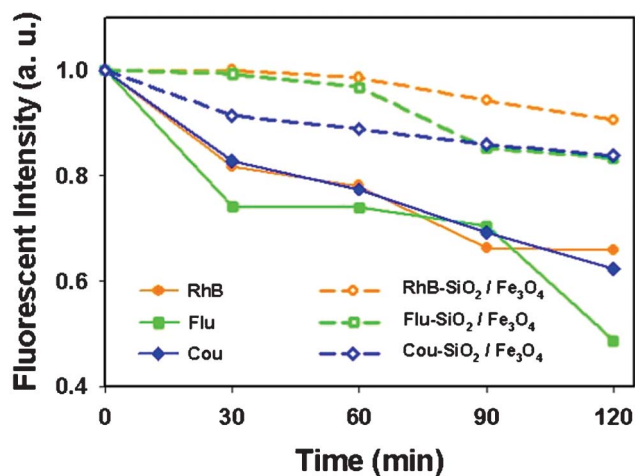


**Fig. 5** Results from photostability tests of RhB, Flu, Cou, RhB-SiO<sub>2</sub>-Fe<sub>3</sub>O<sub>4</sub>, Flu-SiO<sub>2</sub>-Fe<sub>3</sub>O<sub>4</sub>, and Cou-SiO<sub>2</sub>-Fe<sub>3</sub>O<sub>4</sub>. The plot provides fluorescent intensity versus time of exposure to the light of a mercury discharge lamp. All samples were dispersed in ethanol.

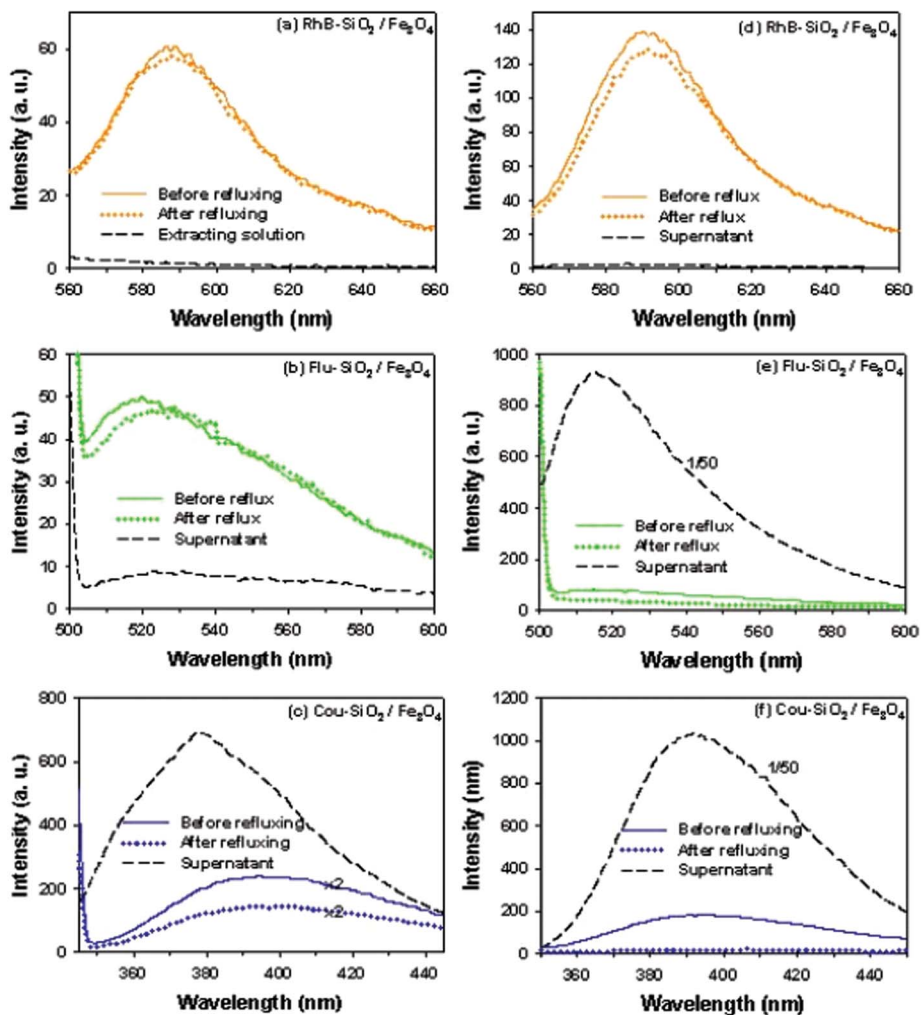


**Fig. 6** Emission spectra of (a) RhB-SiO<sub>2</sub>-Fe<sub>3</sub>O<sub>4</sub>, (b) Flu-SiO<sub>2</sub>-Fe<sub>3</sub>O<sub>4</sub>, and (c) Cou-SiO<sub>2</sub>-Fe<sub>3</sub>O<sub>4</sub>, before and after refluxing with ethanol along with that of their supernatant solutions. Emission spectra of (d) RhB-SiO<sub>2</sub>-Fe<sub>3</sub>O<sub>4</sub>, (e) Flu-SiO<sub>2</sub>-Fe<sub>3</sub>O<sub>4</sub>, and (f) Cou-SiO<sub>2</sub>-Fe<sub>3</sub>O<sub>4</sub>, before and after refluxing with water and that of their supernatant solutions. Additional details for (e) and (f) can be found in Fig. S3 of the ESI.†

nanoparticle assembly, then modification of the silica surface to produce a porous interface might further enhance this effect by providing confined spaces for the trialkoxysilane-modified dye bonding sites. However, additional factors such as the efficiency of the bonding of the modified-dye to the

surface, alternative mechanisms for the loss of the dye molecules, and intermolecular interactions between dye molecules related to intramolecular charge distributions might also influence the overall effectiveness of the covalent attachment of these dyes. Further studies will be needed to

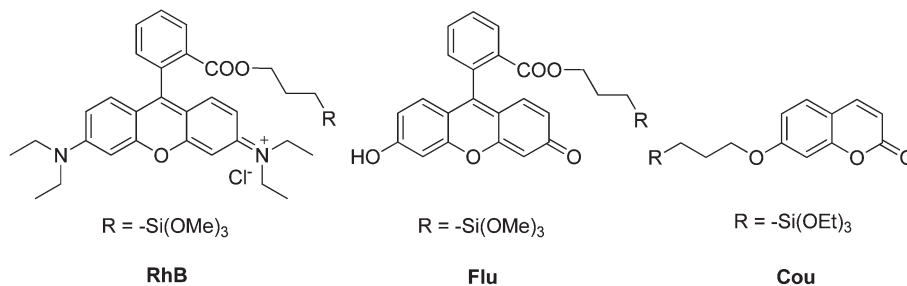


**Fig. 7** Illustrations of the molecular structures for (RhB) the trimethoxysilane-modified rhodamine B dye, (Flu) the trimethoxysilane-modified fluorescein dye, and (Cou) the triethoxysilane-modified 7-hydroxycoumarin dye.

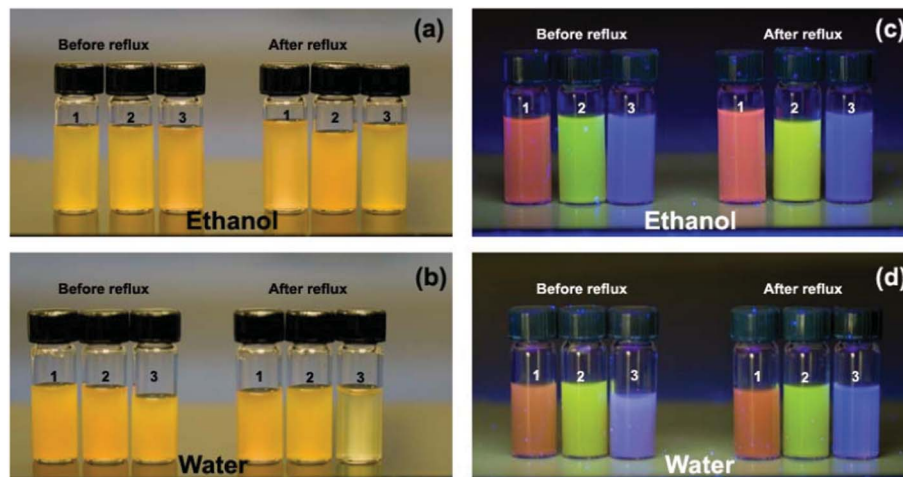


**Fig. 8** Photographs of dye-SiO<sub>2</sub>-Fe<sub>3</sub>O<sub>4</sub> particles in solution: RhB-SiO<sub>2</sub>-Fe<sub>3</sub>O<sub>4</sub> in vial 1, Flu-SiO<sub>2</sub>-Fe<sub>3</sub>O<sub>4</sub> in vial 2; and Cou-SiO<sub>2</sub>-Fe<sub>3</sub>O<sub>4</sub> in vial 3, before and after reflux in ethanol (a) and (c), and water (b) and (d). The images shown in (a) and (b) were taken under white light while those in (c) and (d) were taken under a UV lamp.

define the structural parameters needed to produce the most stable dye-SiO<sub>2</sub>-Fe<sub>3</sub>O<sub>4</sub> nanoparticle assembly.

The photographs in Fig. 8a and 8b (taken under white light) show the dye-SiO<sub>2</sub>-Fe<sub>3</sub>O<sub>4</sub> nanoparticles suspended in ethanol before and after refluxing for 24 h in ethanol and in water. There is a noticeable reduction in the presence of the Cou-SiO<sub>2</sub>-Fe<sub>3</sub>O<sub>4</sub> nanoparticles in the vial associated with the nanoparticles collected by centrifugation after performing a 24 h reflux in water. The photographs in Fig. 8c and 8d (taken under a UV lamp) show the dye-SiO<sub>2</sub>-Fe<sub>3</sub>O<sub>4</sub> nanoparticles suspended in ethanol before and after refluxing for 24 h in ethanol and in water, respectively. These photographs exhibit the emission colors of the dye-SiO<sub>2</sub>-Fe<sub>3</sub>O<sub>4</sub> nanoparticles. Although they have been exposed to an elevated temperature for an extended period of time in a potentially reactive solvent, the emission colors of the dye-SiO<sub>2</sub>-Fe<sub>3</sub>O<sub>4</sub> remain vividly bright. The differences between the before-and-after images are not easily distinguished by the eye, but readily measurable

with a spectrometer. Overall, these results indicate that the modified fluorescent dye molecules can be designed to remain chemically embedded in the silica matrix and resistant to detachment, thus yielding brilliant and stable fluorescent signals for biological studies. It is also worth noting here that the dye-SiO<sub>2</sub>-Fe<sub>3</sub>O<sub>4</sub> nanoparticles disperse well in both ethanol and aqueous solution without any precipitation.

In separate studies, the Flu-SiO<sub>2</sub>-Fe<sub>3</sub>O<sub>4</sub> nanoparticles were placed in aqueous solution at several pH values to demonstrate both the dispersibility and stability of the dye-SiO<sub>2</sub>-Fe<sub>3</sub>O<sub>4</sub> nanoparticle structure when exposed to acidic and basic conditions. The results for this set of experiments are provided in the supporting information (see Fig. S4, ESI†). The observed high stabilities in neutral and basic ranges can be attributed to the absence of amine terminal groups existing on the surface of the nanoparticles<sup>47,49,50</sup> which are unlike other magnetic-

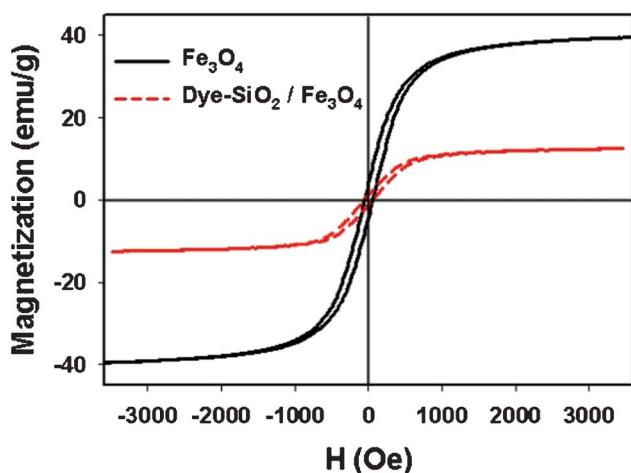


**Fig. 9** Room temperature magnetic hysteresis curves of Fe<sub>3</sub>O<sub>4</sub> and dye-SiO<sub>2</sub>-Fe<sub>3</sub>O<sub>4</sub> nanoparticles, where dye = RhB.

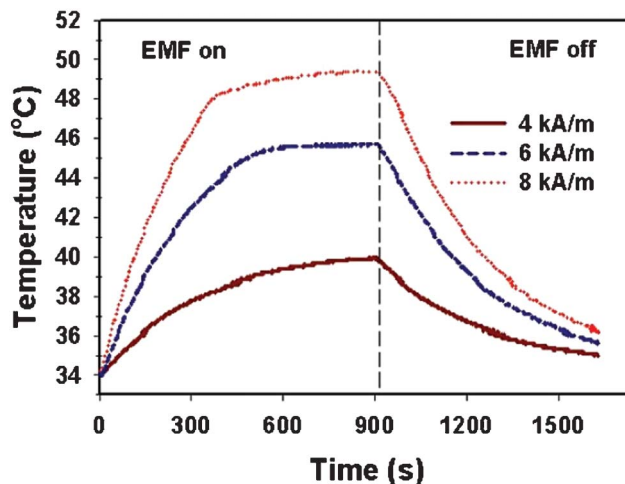


**Fig. 10** Change in temperature of RhB-SiO<sub>2</sub>-Fe<sub>3</sub>O<sub>4</sub> nanoparticles in aqueous solution at a concentration of 40 mg mL<sup>-1</sup> Fe<sub>3</sub>O<sub>4</sub> as a function of time under magnetic field strengths of 4, 6, and 8 kA m<sup>-1</sup> at 100 kHz.

fluorescent nanoparticles prepared using APTES and isothiocyanate-modified dye molecules.

### Magnetic properties of dye-SiO<sub>2</sub>-Fe<sub>3</sub>O<sub>4</sub> nanoparticles

The magnetic properties of the nanoparticle samples were evaluated using a vibrating sample magnetometer (VSM). Fig. 9 shows the magnetic hysteresis at room temperature for as-prepared Fe<sub>3</sub>O<sub>4</sub> and RhB-SiO<sub>2</sub>-Fe<sub>3</sub>O<sub>4</sub> nanoparticles, with saturation magnetization of 39.6 and 12.5 emu g<sup>-1</sup>, respectively. The saturation magnetization decreases due to the presence of the nonmagnetic dye-doped silica shell. Magnetic nanoparticles with high magnetization and low coercivity are crucial for magnetic hyperthermia applications to achieve sufficient heating with a minimum dose of nanoparticles, which avoids possible complications due to iron overload in the body.

We also investigated the heating ability of these magnetic fluorescent nanoparticle colloids for possible use as therapeutic agents in hyperthermia applications. Induction heating of the aqueous solution of RhB-SiO<sub>2</sub>-Fe<sub>3</sub>O<sub>4</sub> nanoparticles at a concentration of 40 mg mL<sup>-1</sup> was conducted at 100 kHz in applied fields ranging from 4 to 8 kA m<sup>-1</sup>. The change in temperature as a function of time at various magnetic field strengths is plotted in Fig. 10. The data show that the temperature increases more rapidly when a higher magnetic field is applied, while heating experiments using only deionized water did not show any significant temperature increase (*i.e.*, the temperature change was less than 0.2 °C; data not shown). The heating profile of the RhB-SiO<sub>2</sub>-Fe<sub>3</sub>O<sub>4</sub> nanoparticles under oscillating magnetic fields shows that the hybrid nanoparticles are suitable for hyperthermia applications as the therapeutic temperature range for killing tumor cells is 42–46 °C.<sup>76</sup>

Fig. 11 shows the magnetic susceptibility images of a dry sample of RhB-SiO<sub>2</sub>-Fe<sub>3</sub>O<sub>4</sub> particles (top) and a dry sample of commercial nanomag<sup>®</sup>-D particles described in the experimental section (bottom) taken at 2 kHz. Despite the smaller

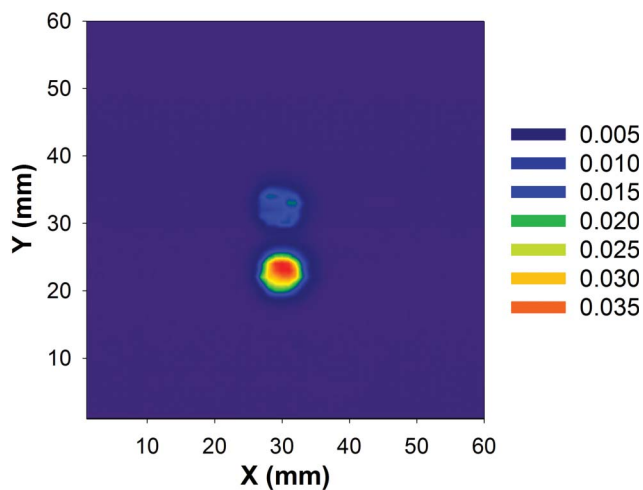


**Fig. 11** Magnetic susceptibility images of a RhB-SiO<sub>2</sub>-Fe<sub>3</sub>O<sub>4</sub> sample (200 µg) and a commercial nanomag<sup>®</sup>-D sample (200 µg), located at x,y = 30;33 and 30;23, respectively.

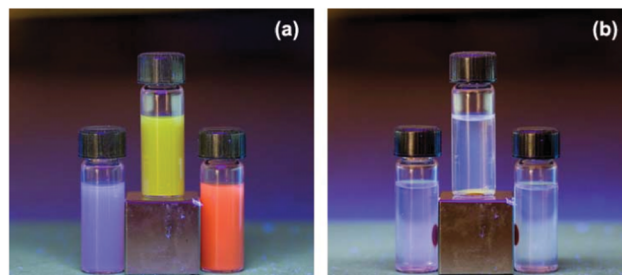


**Fig. 12** The emission color of the dye-SiO<sub>2</sub>-Fe<sub>3</sub>O<sub>4</sub> nanoparticles under UV light irradiation (a) dispersed in solution and (b) after magnetic capture, where the dyes are Cou, Flu, and RhB (left to right, respectively). This demonstration verifies that the modified dyes are covalently attached to the magnetic SiO<sub>2</sub>-Fe<sub>3</sub>O<sub>4</sub> nanoparticles.

magnetic susceptibility of our custom-designed nanoparticles, a spatially resolved image was readily obtained. This comparison demonstrates the potential utility of dye-SiO<sub>2</sub>-Fe<sub>3</sub>O<sub>4</sub> nanoparticles for sentinel lymph node mapping and magnetic nanoparticle-guided surgery using a hand-held magnetic probe.

The photograph in Fig. 12 illustrates both the magnetic and fluorescent properties of the dye-SiO<sub>2</sub>-Fe<sub>3</sub>O<sub>4</sub> nanoparticles. Under UV light, the samples emit different colors produced by the incorporated dyes in the corresponding silica matrix. Once a rare earth magnet ( $B_m \sim 1T$ ) was placed close to the vials filled with these colloids, the nanoparticles were completely separated to one side of the vial within minutes, thereby leaving a clear and transparent buffer solution. This demonstration highlights the effectiveness of combining optical and magnetic properties in one system. The nanoparticles were readily re-dispersed into solution either by gently shaking or sonicating the vial. This experiment also confirms that the dyes that are covalently attached to the nanoparticles are the source of the emitted light, and not dyes dissolved in solution.

## Conclusions

We have established a simple and controllable method for the synthesis of composite nanoparticles consisting of a Fe<sub>3</sub>O<sub>4</sub> core and a dye-doped porous SiO<sub>2</sub> shell. These versatile composite nanoparticles are dispersible in aqueous solutions, offer a dynamic response to an external magnetic field, and produce bright fluorescent emissions. The stability of the dye-SiO<sub>2</sub>-Fe<sub>3</sub>O<sub>4</sub> nanoparticle assemblies were tested under the harsh conditions of both a 24-hour reflux in water and ethanol, yielding a conclusion that structural parameters of the attached dye contribute to the observed relative stability for these assemblies: RhB-SiO<sub>2</sub>-Fe<sub>3</sub>O<sub>4</sub> > Flu-SiO<sub>2</sub>-Fe<sub>3</sub>O<sub>4</sub> > Cou-SiO<sub>2</sub>-Fe<sub>3</sub>O<sub>4</sub>. The outstanding properties of these composite nanoparticles, their high magnetization, variety of fluorescent signals, and unique dispersive character in a variety of acid/base environments, make them useful for a myriad of biomedical applications, not only as multi-modal contrast agents, but also as therapeutic agents.

## Acknowledgements

We thank the National Science Foundation (ECCS-0926027), the Robert A. Welch Foundation (Grant No. E-1320), the Alliance for NanoHealth (W81XWH-10-2-0125), and the Texas Center for Superconductivity at the University of Houston for generous financial support.

## References

- J. V. Frangioni, *Curr. Opin. Chem. Biol.*, 2003, **7**, 626–634.
- W. Li, X. Yang, K. Wang, W. Tan, Y. He, Q. Guo, H. Tang and J. Liu, *Anal. Chem.*, 2008, **80**, 5002–5008.
- J. S. Guthi, S.-G. Yang, G. Huang, S. Li, C. Khemtong, C. W. Kessinger, M. Peyton, J. D. Minna, K. C. Brown and J. Gao, *Mol. Pharmaceutics*, 2010, **7**, 32–40.
- A. Heymer, D. Haddad, M. Weber, U. Gbureck, P. M. Jakob, J. Eulert and U. Noeth, *Biomaterials*, 2008, **29**, 1473–1483.
- J.-H. Lee, M. A. Smith, W. Liu, E. M. Gold, B. Lewis, H.-T. Song and J. A. Frank, *Nanotechnology*, 2009, **20**, 355102.
- A. Stroh, J. Boltze, K. Sieland, K. Hild, C. Gutzeit, T. Jung, J. Kressel, S. Hau, D. Reich, T. Grune and C. Zimmer, *Mol. Imaging*, 2009, **8**, 166–178.
- J. Weizenecker, B. Gleich, J. Rahmer, H. Dahnke and J. Borgert, *Phys. Med. Biol.*, 2009, **54**, L1–L10.
- B. Gleich and J. Weizenecker, *Nature*, 2005, **435**, 1214–1217.
- S. Sarangi, I. C. Tan and A. Brazdeikis, *J. Appl. Phys.*, 2009, **105**, 093926.
- E. R. Flynn and H. C. Bryant, *Phys. Med. Biol.*, 2005, **50**, 1273–1293.
- T. Nakagawa, Y. Minamiya, Y. Katayose, H. Saito, K. Taguchi, H. Imano, H. Watanabe, K. Enomoto, M. Sageshima, T. Ueda and J.-i. Ogawa, *J. Thorac. Cardiovasc. Surg.*, 2003, **126**, 563–567.
- L. Johnson, G. Charles-Edwards and M. Douek, *Cancers*, 2010, **2**, 1884–1894.
- M. G. Harisinghani, J. Barentsz, P. F. Hahn, W. M. Deserno, S. Tabatabaei, C. H. van de Kaa, J. de la Rosette and R. Weissleder, *N. Engl. J. Med.*, 2003, **348**, 2491–2499.
- J. Cheon and J. H. Lee, *Acc. Chem. Res.*, 2008, **41**, 1630–1640.
- M. F. Kircher, U. Mahmood, R. S. King, R. Weissleder and L. Josephson, *Cancer Res.*, 2003, **63**, 8122–8125.
- J.-H. Park, G. V. Maltzahn, E. Ruoslahti, S. N. Bhatia and M. J. Sailor, *Angew. Chem., Int. Ed.*, 2008, **47**, 7284–7288.
- S. P. Foy, R. L. Manthe, S. T. Foy, S. Dimitrijevic, N. Krishnamurthy and V. Labhassetwar, *ACS Nano*, 2010, **4**, 5217–5224.
- N. Chekina, D. Horak, P. Jendelova, M. Trchova, M. J. Benes, M. Hruby, V. Herynek, K. Turnovcova and E. Sykova, *J. Mater. Chem.*, 2011, **21**, 7630–7639.
- F. Wang, X.-L. Chen, Z.-X. Zhao, S.-H. Tang, X.-Q. Huang, C.-H. Lin, C.-b. Cai and N.-F. Zheng, *J. Mater. Chem.*, 2011, **21**, 11244–11252.
- J. Kim, H. S. Kim, N. Lee, T. Kim, H. Kim, T. Yu, I. C. Song, W. K. Moon and T. Hyeon, *Angew. Chem., Int. Ed.*, 2008, **47**, 8438–8441.
- O. Rodriguez, S. Fricke, C. Chien, L. Dettin, J. v. Meter, E. Shapiro, H. N. Dai, M. Casimiro, L. Ileva, J. Dagata, M. D. Johnson, M. P. Lisanti, A. Koretsky and C. Albanese, *Cell Cycle*, 2006, **5**, 113–119.
- Y. Sahoo, A. Goodarzi, M. T. Swihart, T. Y. Ohulchanskyy, N. Kaur, E. P. Furlani and P. N. Prasad, *J. Phys. Chem. B*, 2005, **109**, 3879–3885.
- A. G. J. Tibbe, B. G. de Groot, J. Greve, P. A. Liberti, G. J. Dolan and L. W. M. M. Terstappen, *Nat. Biotechnol.*, 1999, **17**, 1210–1213.
- G. P. Wang, E. Q. Song, H. Y. Xie, Z. L. Zhang, Z. Q. Tian, C. Zuo, D. W. Pang, D. C. Wu and Y. B. Shi, *Chem. Commun.*, 2005, 4276–4278.
- H. Y. Xie, C. Zuo, Y. Liu, Z. L. Zhang, D. W. Pang, X. L. Li, J. P. Gong, C. Dickinson and W. C. Zhou, *Small*, 2005, **1**, 506–509.
- T.-J. Yoon, K. N. Yu, E. Kim, J. S. Kim, B. G. Kim, S.-H. Yun, B.-H. Sohn, M. H. Cho, J.-K. Lee and S. B. Park, *Small*, 2006, **2**, 209–215.
- D.-Y. Chen, M.-J. Jiang, N.-J. Li, H.-W. Gu, Q.-F. Xu, J.-F. Ge, X.-W. Xia and J.-M. Lu, *J. Mater. Chem.*, 2010, **20**, 6422–6429.
- L. Levy, Y. Sahoo, K. S. Kim, E. J. Bergey and P. N. Prasad, *Chem. Mater.*, 2002, **14**, 3715–3721.
- Y. M. Huh, Y. W. Jun, H. T. Song, S. Kim, J. S. Choi, J. H. Lee, S. Yoon, K. S. Kim, J. S. Shin, J. S. Suh and J. Cheon, *J. Am. Chem. Soc.*, 2005, **127**, 12387–12391.
- W. Zhang, Y. Zhang, X. Shi, C. Liang and Y. Xian, *J. Mater. Chem.*, 2011, **21**, 16177–16183.
- Y. Song, C. Zhao, J. Ren and X. Qu, *Chem. Commun.*, 2009, 1975–1977.
- J. Kim, J. E. Lee, J. Lee, J. H. Yu, B. C. Kim, K. An, Y. Hwang, C. H. Shin, J. G. Park, J. Kim and T. Hyeon, *J. Am. Chem. Soc.*, 2006, **128**, 688–689.
- J. Choi, J. C. Kim, Y. B. Lee, I. S. Kim, Y. K. Park and N. H. Hur, *Chem. Commun.*, 2007, **16**, 1644–1646.
- Y. Okamoto, F. Kitagawa and K. Otsuka, *Anal. Chem.*, 2007, **79**, 3041–3047.
- D. K. Yi, S. T. Selvan, S. S. Lee, G. C. Papaefthymiou, J. Y. Kundaliya and J. Ying, *J. Am. Chem. Soc.*, 2005, **127**, 4990–4991.
- F. Bertorelle, C. Wilhelm, J. Roger, F. Gazeau, C. Menager and V. Cabuil, *Langmuir*, 2006, **22**, 5385–5391.
- H. W. Gu, K. M. Xu, Z. M. Yang, C. K. Chang and B. Xu, *Chem. Commun.*, 2005, 4270–4272.
- N. Nitin, L. E. W. Laconte, O. Zurkiya, X. Hu and G. Bao, *J. Biol. Inorg. Chem.*, 2004, **9**, 706–712.
- G. Li, D. L. Zeng, L. Wang, B. Zong, K. G. Neoh and E. T. Kang, *Macromolecules*, 2009, **42**, 8561–8565.
- Y.-S. Lin, S.-H. Wu, Y. Hung, Y.-H. Chou, C. Chang, M.-L. Lin, C.-P. Tsai and C.-Y. Mou, *Chem. Mater.*, 2006, **18**, 5170–5172.
- A. Abou-Hassan, R. Bazzi and V. Cabuil, *Angew. Chem., Int. Ed.*, 2009, **48**, 7180–7183.
- Q. Chang, L. Zhu, C. Yu and H. Tang, *J. Lumin.*, 2008, **128**, 1890–1895.
- J. Wan, X. Meng, E. Liu and K. Chen, *Nanotechnology*, 2010, **21**, 235104.
- M. Stjernedahl, M. Andersson, H. E. Hall, D. M. Pajerowski, M. W. Meisel and R. S. Duran, *Langmuir*, 2008, **24**, 3532–3536.
- P. Sharma, S. Brown, G. Walter, S. Santra and B. Moudgil, *Adv. Colloid Interface Sci.*, 2006, **123–126**, 471–485.

- 46 C. Sanchez, B. Julián, P. Belleville and M. Popall, *J. Mater. Chem.*, 2005, **15**, 3559–3592.
- 47 A. van Blaaderen and A. Vrij, *Langmuir*, 1992, **8**, 2921–2931.
- 48 S. Santra, P. Zhang, K. Wang, R. Tapeç and W. Tan, *Anal. Chem.*, 2001, **73**, 4988–4993.
- 49 Q. A. Pankhurst, J. Connolly, S. K. Jones and J. Dobson, *J. Phys. D: Appl. Phys.*, 2003, **36**, R167–R181.
- 50 M. Levy, A. Quarta, A. Espinosa, A. Figuerola, C. Wilhelm, M. Garcia-Hernandez, A. Genovese, A. Falqui, D. Alloyeau, R. Buonsanti, P. D. Cozzoli, M. A. Garcia, F. Gazeau and T. Pellegrino, *Chem. Mater.*, 2011, **23**, 4170–4180.
- 51 R. Hergt, S. Dutz, R. Mueller and M. Zeisberger, *J. Phys.: Condens. Matter*, 2006, **18**, S2919–S2934.
- 52 P. Moroz, S. K. Jones and B. N. Gray, *J. Surg. Oncol.*, 2002, **80**, 149–156.
- 53 P. Moroz, S. K. Jones and B. N. Gray, *Int. J. Hyperthermia*, 2002, **18**, 267–284.
- 54 P. Moroz, S. K. Jones and B. N. Gray, *J. Surg. Res.*, 2002, **105**, 209–214.
- 55 P. Moroz, H. Pardoe, S. K. Jones, T. G. St. Pierre, S. Song and B. N. Gray, *Phys. Med. Biol.*, 2002, **47**, 1591–1602.
- 56 P. Moroz, S. K. Jones, C. Metcalf and B. N. Gray, *Int. J. Hyperthermia*, 2003, **19**, 23–34.
- 57 M. Shinkai, B. Le, H. Honda, K. Yoshikawa, K. Shimizu, S. Saga, T. Wakabayashi, J. Yoshida and T. Kobayashi, *Cancer Sci.*, 2001, **92**, 1138–1145.
- 58 K. J. Widder, R. M. Morris, G. Poore, D. P. Howard, Jr. and A. E. Senyei, *Proc. Natl. Acad. Sci. U. S. A.*, 1981, **78**, 579–581.
- 59 U. O. Hafeli, S. M. Sweeney, B. A. Beresford, J. L. Humm and R. M. Macklis, *Nucl. Med. Biol.*, 1995, **22**, 147–155.
- 60 F. Wiekhorst, C. Seliger, R. Jurgons, U. Steinhoff, D. Eberbeck, L. Trahms and C. Alexiou, *J. Nanosci. Nanotechnol.*, 2006, **6**, 3222–3225.
- 61 T. Kato, R. Nemoto, H. Mori, R. Abe, K. Unno, A. Goto, H. Murota, M. Harada and M. Homma, *Appl. Biochem. Biotechnol.*, 1984, **10**, 199–211.
- 62 Y. Morimoto, K. Sugibayashi, M. Okumura and Y. Kato, *J. Pharmacobio-Dyn.*, 1980, **3**, 264–267.
- 63 P. K. Gupta, C. T. Hung and N. S. Rao, *J. Pharm. Sci.*, 1989, **78**, 290–294.
- 64 K. J. Widder, A. E. Senyei and D. G. Scarpelli, *Proc. Soc. Exp. Biol. Med.*, 1978, **158**, 141–146.
- 65 T. Hoare, J. Santamaria, G. F. Goya, S. Irusta, D. Lin, S. Lau, R. Padera, R. Langer and D. S. Kohane, *Nano Lett.*, 2009, **9**, 3651–3657.
- 66 R. J. Mart, K. P. Liem and S. J. Webb, *Chem. Commun.*, 2009, 2287–2289.
- 67 R. Regmi, S. R. Bhattarai, C. Sudakar, A. S. Wani, R. Cunningham, P. P. Vaishnava, R. Naik, D. Oupicky and G. Lawes, *J. Mater. Chem.*, 2010, **20**, 6158–6163.
- 68 S.-H. Ha, C. E. Camalier, G. R. Beck Jr and J.-K. Lee, *Chem. Commun.*, 2009, 2881–2883.
- 69 H. Deng, X. Li, Q. Peng, X. Wang, J. Chen and Y. Li, *Angew. Chem., Int. Ed.*, 2005, **44**, 2782–2785.
- 70 W. Stöber, A. Fink and E. Bohn, *J. Colloid Interface Sci.*, 1968, **26**, 62–69.
- 71 J. Ge, Q. Zhang, T. Zhang and Y. Yin, *Angew. Chem., Int. Ed.*, 2008, **47**, 8924–8928.
- 72 I. Sokolov and D. O. Volkov, *J. Mater. Chem.*, 2010, **20**, 4247–4250.
- 73 Q. Zhang, J. Ge, J. Goebel, Y. Hu, Y. Sun and Y. Yin, *Adv. Mater.*, 2010, **22**, 1905–1909.
- 74 S. A. Corr, Y. P. Rakovich and Y. K. Gun'ko, *Nanoscale Res. Lett.*, 2008, **3**, 87–104.
- 75 N. O. Mchedlov-Petrosyan and Y. V. Kholin, *Russ. J. Appl. Chem.*, 2004, **77**, 414–422.
- 76 D. C. Chan, D. B. Kirpotin and P. A. J. Bunn, *Scientific and clinical applications of magnetic carriers*, Premium Press, New York, 1997.